npj | digital medicine

Article

Published in partnership with Seoul National University Bundang Hospital

https://doi.org/10.1038/s41746-025-01736-6

Multiscale modeling of drug-induced liver injury from organ to lobule

Check for updates

Alon Malka-Markovitz[1], Stelian Camara Dit Pinto[1], Mohammed Cherkaoui[1], Steven M. Levine[2], Sharmila Anandasabapathy[3], Gagan K. Sood[3], Sadhna Dhingra[4], Gao Yujia[5], John M. Vierling[3] & Nicolas R. Gallo[1,6] ✉

Drug-induced liver injury poses significant challenges in drug development and in clinical care. This study builds on prior work developing a Human Liver Virtual Twin by creating a Multiscale Computational Fluid Dynamics framework that integrates patient-specific anatomical data to predict acetaminophen-induced liver injury as a demonstration of its capability. The model bridges vascular, lobular, and cellular scales to simulate dynamic blood flow, drug transport, and injury mechanisms that accurately reflect clinically observed spatial heterogeneity. Results demonstrate accurate blood flow dynamics, predictions of hepatocellular damage, and a scalable framework for studying spatial heterogeneity applicable to other hepatic pathologies. This work establishes the foundational principles for a whole-organ virtual liver simulation methodology, potentially becoming a powerful tool to guide safety in therapeutic development and clinical treatment strategies, ultimately reducing reliance translation from animal models for preclinical drug testing.

Drug-induced liver injury (DILI) is a significant risk to patient health and a major burden on our healthcare system by negatively impacting both drug development, regulatory approval and post-market clinical management. DILI can either be intrinsic, which is dose-dependent and predictable or idiosyncratic, which is unpredictable and not dose-dependent. Idiosyncratic DILI can be mediated by immunological or non-immunological mechanisms and the diagnosis often requires exclusion of other etiologies of liver disease[1]. DILI is a leading cause of attrition during clinical drug development and a primary reason for post-approval withdrawal of drugs from the market[2–4]. The infrequency and unpredictability of idiosyncratic DILI is especially problematic because of the low probability of detection during preclinical and early clinical testing[2–4]. The inability of in vitro and animal models to identify human-specific toxic responses prevents detection idiosyncratic DILI until hepatotoxic adverse events occur in clinical stages of development[5–10].

One novel solution to the inadequacies of in vitro and animal testing during preclinical drug development would be a human liver virtual twin (HLVT) that can accurately depict human hepatic physiology and dynamic responses involving drug Absorption, Distribution, Metabolization, and Excretion (ADME). Such a HLVT would be comprised of coupled computational models that mimic the structure, function, and responses of a normal human liver. Combining data from imaging, genetics, and clinical data, HLVTs could provide patient or population specific surrogate livers suitable for functional simulations, enabling more precise diagnosis, treatment planning, and predictable drug testing[11]. Indeed, other organ-level VTs have shown promise as replacement for animal or organoid models by providing additional human-specific insights on liver dynamics for the development of novel therapies in various areas of medicine[12–19], stimulating multiple ongoing efforts toward building and validating human organ VTs[20–25].

Through our development plan for the Living Liver[11] virtual twin, our approach is to systematically build a HLVT capable of predicting idiosyncratic DILI in a stepwise fashion, validating its accuracy at each step. At this time, a focus directly on idiosyncratic DILI is premature given the incomplete understanding of the pathogenesis of specific idiosyncratic drugs. A clearer clinical foundation will be required to model and validate the physiological and biochemical phenomena across scales ranging from the cellular, tissue, and organ levels[11,26,27]. Thus, we have sought to build a strong methodological foundation by first modeling a well-characterized yet clinically significant dose-dependent DILI.

Since hemodynamic variations are believed to be a major source of DILI's spatial heterogeneity, we will use this as a proxy for propensity for DILI. It is believed that heterogeneous blood flow contributes to difference in drug distribution and hepatotoxicity distribution over the whole organ[28].

[1]Center of Excellence, Long Island University, Brooklyn, NY, USA. [2]Dassault Systèmes, Vélizy-Villacoublay, France. [3]Departments of Medicine and Surgery, Baylor College of Medicine, Houston, TX, USA. [4]Department of Pathology and Genomic Medicine, Houston Methodist Hospital, Houston, TX, USA. [5]Department of Surgery, National University Hospital, National University Health System, Singapore, Singapore. [6]School of Digital Engineering, Computer Science and Artificial Intelligence, Long Island University, Brooklyn, NY, USA. ✉e-mail: nicolas.gallo@liu.edu

Such hemodynamic-driven heterogeneity has been observed in various liver diseases[29–32] and during targeted drug delivery applications[33–35]. EASL clinical guidelines for DILI reviewed in 2022 highlight how perfusion abnormalities due to previous injury may relate to the zonal heterogeneity of DILI, particularly in conditions where liver architecture and blood flow influence the distribution of hepatotoxic agents[36]. The guidelines suggest that abnormal perfusion, due to altered blood supply or vascular changes, contributes to the distribution of damage across different liver zones. Altered perfusion impacts the zonal distribution of Kupffer cells and monocyte-derived macrophages, leading to localized areas of increased inflammation or fibrosis, typically in regions with specific perfusion characteristics, such as pericentral zones[37].

Dose-dependent APAP-induced liver injury (AILI) was chosen for this study due to its clinical and economic significance, as it is the most common cause of both acute liver injury and potentially fatal acute liver failure[1,38]. Currently in the U.S., AILI causes >50% of cases of acute liver failure[39,40], accounts for 20% of liver transplants performed for acute liver failure[40], and costs U.S. healthcare system an estimated $86.9 million[41]. In addition, studies of AILI provide an abundant database of clinical and pathological findings and details about the sequential mechanisms of APAP hepatotoxicity. We note that it is well established that APAP-induced hepatotoxicity is primarily driven by metabolic activation and glutathione depletion, rather than vascular perfusion patterns. While hemodynamic factors may influence drug delivery, they do not play a direct role in the initiation of APAP-induced injury. The vascular model presented here provides a framework for studying DILI scenarios where perfusion dynamics are more relevant, such as fibrosis-associated changes in blood flow resistance.

Our prior publication focused on a virtual model of AILI within the hepatic lobule, the fundamental functional unit of the liver. This is needed to create an accurate model that integrates the kinetics of APAP metabolism in different zones of the lobule and multi-spatial scales encompassing molecular, cellular, tissue, and organ levels[11]. Pathological data from clinical cases of human AILI were used to accurately predict the kinetics of AILI, as measured by the onset of hepatocellular necrosis in central lobular zone 3 hepatocytes. The model assumed necrosis was the result of hemodynamic and metabolic differences along the portal vein-central vein axis of cords of hepatocytes[38].

This study builds on that prior work by coupling macro-scale portal hemodynamics with the previously developed virtual hepatic lobule[11]. This is sufficient to begin exploration of patient-specific spatial heterogeneity of DILI within the whole organ. As such, it provides the foundation for predicting severity in individuals with AILI by capturing both the multi-scale, 3D spatial organization of the liver and resulting liver hemodynamics. This is achieved by bridging the organ-level phenomena with their cellular and sub-cellular origins that are necessary for predicting hepatotoxic severity. This novel approach complements and extends existing statistical or Physiologically Based Pharmacokinetic (PBPK) approaches that cannot capture the multi-scale structure and physiological hepatic processes.

Modeling liver dynamics at the lobular scale has significantly advanced our understanding of DILI. These efforts have primarily focused on simulating the microcirculation within liver sinusoidal networks to approximate localized hepatic function. Hexagonal porous media models are commonly used for simulating blood flow within lobules, evolving from simple 2D geometries to more complex representations incorporating isotropic and anisotropic permeabilities[42–47]. Studies of metabolic zonation have demonstrated how differences in enzymatic activity across periportal and pericentral zones influence injury patterns[48–50]. Additionally, research on blood flow obstructions has emphasized the importance of lobular network connectivity in shaping patterns of injury[48]. We recently published the first iteration of the virtual lobule, which integrates hemodynamics spanning from the portal triad to the central vein with APAP metabolism and hepatocyte injury[11]. When applied to a retrospective patient cohort, it demonstrated injury patterns consistent with general histopathological observations. However, while these models offer valuable insights into lobular-scale phenomena, the lack of integration with the broader vascular dynamics limits their ability to simulate organ-level processes comprehensively.

Separately, modeling hepatic perfusion at the organ scale have employed Computational Fluid Dynamics (CFD) to explore the effect of anatomical variations on blood flow and drug distribution. For instance, studies have demonstrated how vascular septa and anisotropic properties of hepatic microvasculature influence portal vein hemodynamics[51,52]. Additionally, porous media models have further captured dynamic flow patterns within microcirculatory networks, enabling improved simulations of drug absorption[53,54]. In vivo validation studies, such as 4D MRI studies, are in good agreement with macro-scale CFD predictions but face challenges in resolving smaller vascular segments due to imaging resolution limitations[55]. Together, these approaches offer insights into perfusion dynamics yet their reliance on static boundary conditions and lack of integration with finer-scale processes limits their applicability in modeling localized DILI.

Efforts to bridge the gap between organ-level and lobular-scale models have focused on multiscale integration frameworks. Techniques such as the Biot-Darcy-Brinkman (BDB) model use homogenization approaches to simulate microcirculation while ensuring computational scalability[56]. Modular systems like those based on the Systems Biology Markup Language (SBML) enable tissue-specific biological parameterization for simulating xenobiotic metabolism[57]. These frameworks have begun to combine systemic pharmacokinetic (PK) models with spatially resolved lobular simulations[51,52,58].

Building on this body of work, the goal of this work was to develop a multiscale liver virtual twin that can integrate patient-specific portal vein anatomy to predict drug diffusion, metabolism, and hepatotoxicity across the liver's vascular hierarchy. To achieve this, we implement a novel integration of large-scale portal vein models derived from MR angiography with surrogate capillary networks and lobule-level sinusoidal blood flow simulations, capturing drug transport dynamics at multiple scales. While the human liver contains approximately 1.5 million lobules, this model uses approximately 100,000 microscale lobule representations. This resolution captures perfusion heterogeneity across the organ while ensuring computational tractability, enabling accurate predictions of localized drug exposure and damage. By exceeding the resolution limits of standard CT and MRI imaging, this approach delivers precise inlet conditions for each lobule and offers a new level of accuracy in predicting DILI within patient-specific liver models

A key innovation of our approach is the comprehensive coupling of these multi-scale components, enabling the use of boundary conditions that dynamically adapt across scales. This framework allows for the incorporation of damage-induced vascular resistance changes, reflecting the evolving hemodynamic impact of DILI. The ability to simulate how vascular boundary conditions evolve in response to changes in lobule health is critical for accurately modeling patient-specific liver injury. By explicitly coupling systemic pharmacokinetics, organ-level perfusion, and cellular-level physiology, our model advances beyond conventional statistical and PBPK methods to provide a mechanistic, spatially resolved framework for predicting localized hepatotoxicity and its potential systemic implications. This work establishes a scalable foundation for future extensions that will incorporate progressive liver injury modeling and dynamically evolving vascular properties, enhancing its potential for personalized medicine applications.

Results

Portal vein simulations were run based on patient specific portal vein geometry generated from segmented images (see Fig. 1). The simulations demonstrated inlet pressures of 1150 ± 50 Pa with inlet flow rates ranging from 9.48 to 11.43 cm^3/s (see Fig. 2), this is with good agreement to the results of Ma et al.[52]. The simulations results can be seen in Fig. 3. Velocity patterns showed non-uniform flow due to complex vein geometry (Fig. 3b), with higher velocities in the central vein bulk and minimal velocities near the wall (Fig. 3c), this is consistent with in vivo measurements using 4D MRI

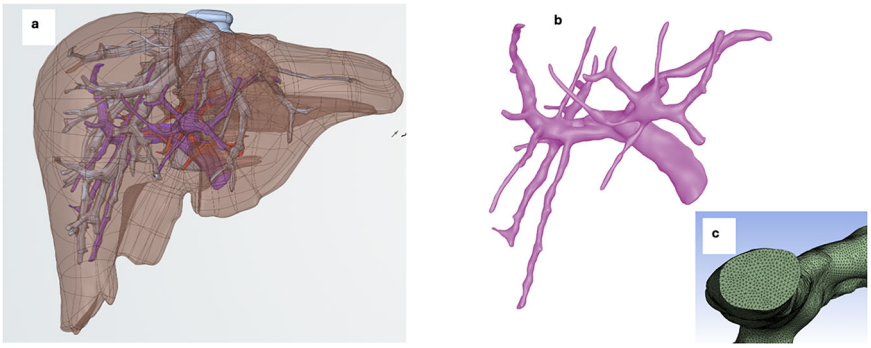


Fig. 1 | Portal vein geometry and meshing. a Full patient-specific liver geometry. **b** Geometry of the patient-specific Portal Vein CFD simulation. **c** Mesh cross-section.

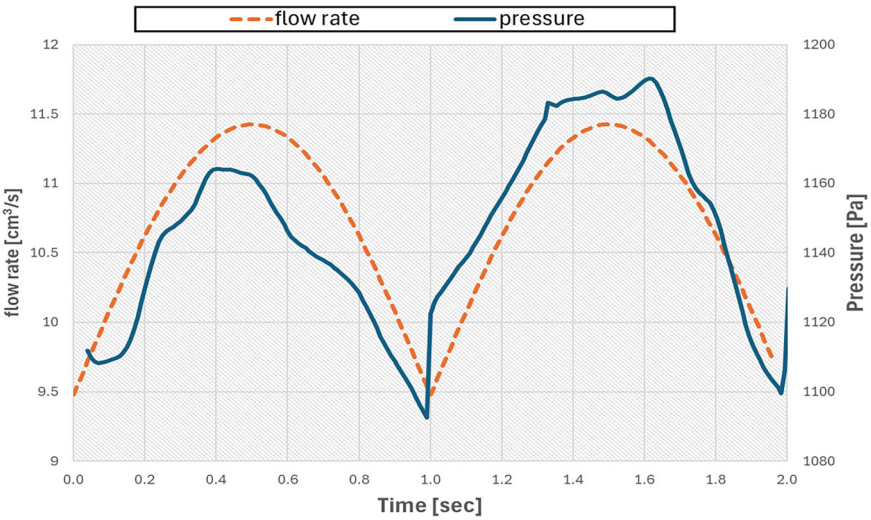


Fig. 2 | Portal vein Blood flow rate and pressure inlet simulation. Time-dependent simulation of portal vein inflow showing pulsatile pressure (blue) and flow rate (dashed orange) over a 2-s cardiac cycle. These dynamic inlet conditions are used to drive downstream liver simulations.

flow, which similarly show irregular flow dynamics in realistic patient models[55] shown in Fig. 4. Outlets exhibited flow rates from 0.6 to 2.1 cm^3/s, with velocities varying between 0.035 ± 0.007 m/s and 0.10 ± 0.02 m/s. The results showed expected APAP transport with a 0.3 × 10^{-3} mass fraction across all 22 outlets.

The effect of drug concentration on flow dynamics was considered to be minimal in our simulations, as changes in concentration do not significantly impact the overall flow behavior. To confirm this, sensitivity simulations at both upper and lower concentration limits were performed and found no noticeable influence on outcomes. Density differences between blood (1.025 g/mL) and APAP (1.260 g/mL) induced minor pressure changes (~10%), deemed negligible under current conditions.

The suggested 2D Capillary Surrogate Model simulations (CSM) were run with the CCO inferred model to join the macro portal veins simulation, and the lobule small size inlet capillaries as illustrated in Fig. 5. As explained above, two consecutive CSM simulations were conducted from Large CSM (from 1.5 mm inlet to 0.3 mm) and small CSM (from 0.3 mm inlet to 0.05 mm outlet).

Large CSM simulations were based on the Portal vein outlet results. High, average, and low resulted inlet velocity showed a similar velocity pattern (see Fig. 6) with different extremum values. The inlet velocities dropped by 16–9% across outlets due to bifurcation and structural changes. All 64 outlets in the simulation received APAP concentration illustrating a healthy capillary structure of smaller veins.

Small CSM followed the same method, the inlet velocities boundary conditions given by the Large CSM. In the small CSM simulations, the outlets boundary conditions are modeled as constant pressure of 800 ± 50 [Pa]. High, average, and low resulted inlet velocity showed similar patterns (see Fig. 7). However, in the case of the Small CSM, the outlets' velocities dropped by 12-8% across outlets due to bifurcation and structural changes. Similarly to the Large CSM, the Small CSM simulation shows that APAP is transported across all outlets. These results of both Large and Small CSM validated the model's scalability and accuracy in capturing microvascular dynamics.

The lobule simulations were divided into two aspects: (1) drug flow delivery simulation and (2) hepatocyte damage model. Lobular drug flow simulations showed inlet velocities from 140 to 1260 μm/s, derived from the CSM outlets, as seen in Fig. 8. Porous media permeability values were fitted and were consistent with literature, averaging 1.25 × 10^{-14} m^2, reflecting a porous medium with 15% sinusoidal tissue and 85% hepatocyte tissue[59]. The average results closely align with those obtained using an 800 Pa pressure inlet in the earlier lobule model. Velocity profiles across the lobule displayed linear relationships with inlet velocities, ranging from 60 to 600 μm/s, in agreement with experimental data[53]. Comparison to Nishii et al.[60] computational validated lobule model achieved similar results as illustrated in Fig. 9. Drug concentrations reached 100% across all nodes, ensuring accurate representation of transport into hepatocytes. Cellular damage model results for average lobule velocity damage induced on the lobular cells following an obtained for a 27.1 g overdose are presented in Fig. 10. The obtained results are consistent with those previously obtained[11] since no change has been made to the lobule mechanical properties (porous media permeability or other) and shown here for completeness.

To further explore the hemodynamic predicting capabilities of the model, we expanded our simulations from acetaminophen-induced liver injury (AILI) to recreating patient-specific condition. The new simulations explored a model of hepatocellular necrosis with injury to liver sinusoidal endothelial cells and/or endothelia of the central veins (i.e., sinusoidal obstructive syndrome) that does result in clinically significant increased

lobular resistance to sinusoidal blood flow. This was examined through synthetic cases simulations having different conditions (increasing vascular outlet pressure to simulate higher blood flow resistance within the lobule). Results for the first scenario show that a 2.5% pressure increase in vascular outlets (from 800 to 820 Pa) is needed to reduce the flow outlet to a negligible velocity (see Fig. 11b) compared to the healthy one (see Fig. 11a). Drug transport becomes negligible in the involved lobules. Conversely, in the second scenario, applying the same 2.5% pressure increase across all outlets (from 800 Pa to 820 Pa) restored drug flow throughout the liver but induces elevated inlet pressures of all the vascular veins by a similar 2.5% (20 Pa) as seen in Fig. 11c. This phenomenon was investigated with various higher pressures (up to 20% increase) and showed similar results. These findings underscore differences in intricate balance between vascular resistance and drug distribution at the lobular level depending on the type and extent of injury and necrosis.

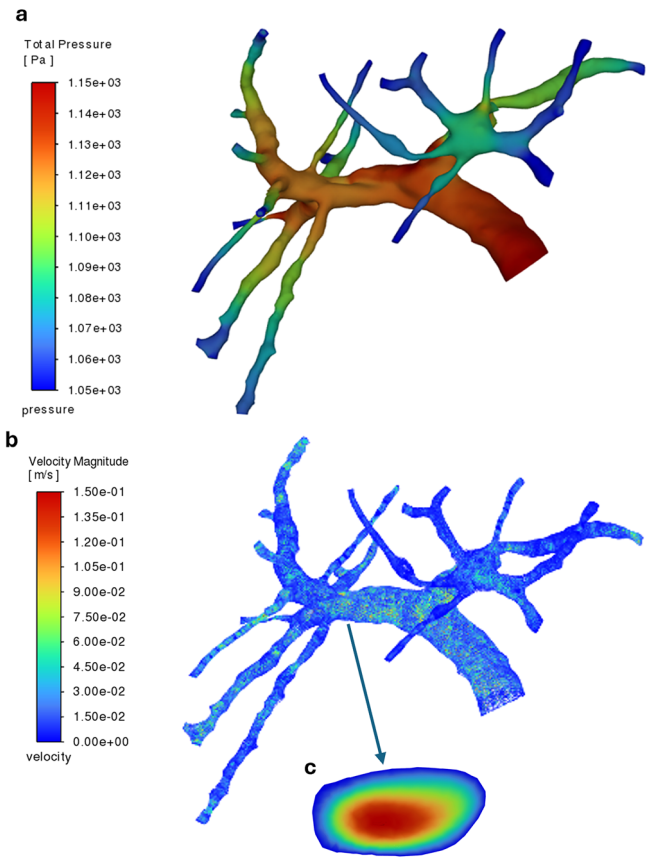


Fig. 3 | Portal vein CFD Simulation results. a Pressure (Pa), (**b**) velocity streamlines (m/s), (**c**) representative cross-section of the velocity gradient in the portal vein.

Discussion

This study presents a comprehensive multiscale model that integrates CFD simulations across the liver's vascular hierarchy, from the lobular to organ scale. Using a dual CSM scheme and tailored boundary conditions, the framework bridges macro- and microscale dynamics, enabling patient-specific predictions of drug distribution, metabolism, and hepatotoxicity. By simulating APAP absorption and flow heterogeneity, the model offers new spatially and temporally resolved insights previously unavailable into drug transport and tissue damage, with potential implications for liver function in both health and disease once rigorous clinical validation is performed.

Portal vein simulations demonstrated strong agreement with previous in silico models[52,61] as well as in vivo measurements using 4D MRI flow[55,62], with velocities around 0.15 m/s. While this validation supports the model's ability to reproduce known conditions, the resolution limits of CT and MRI prevented validation in smaller vascular segments. Simulations also revealed spatial heterogeneity, with lower pressures and velocities observed in the

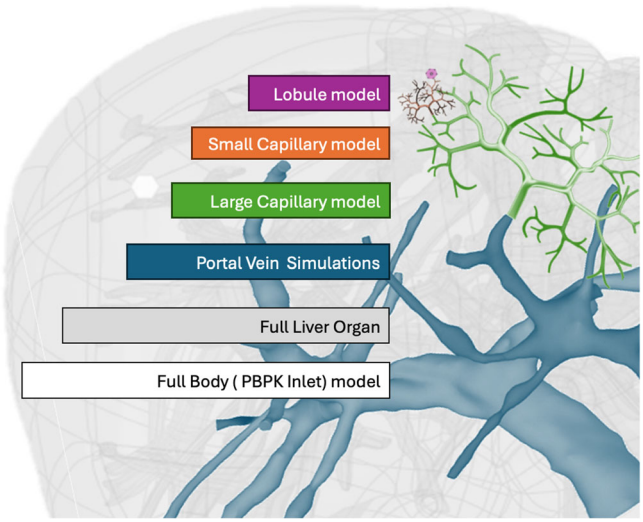


Fig. 5 | A multiscale method scheme. Illustration of the multiscale hierarchical integration of models used to simulate drug transport and toxicity across physiological scales. The framework spans from the full-body PBPK model (bottom) to the lobule model (top), which represents the cellular microenvironment where tissue damage occurs.

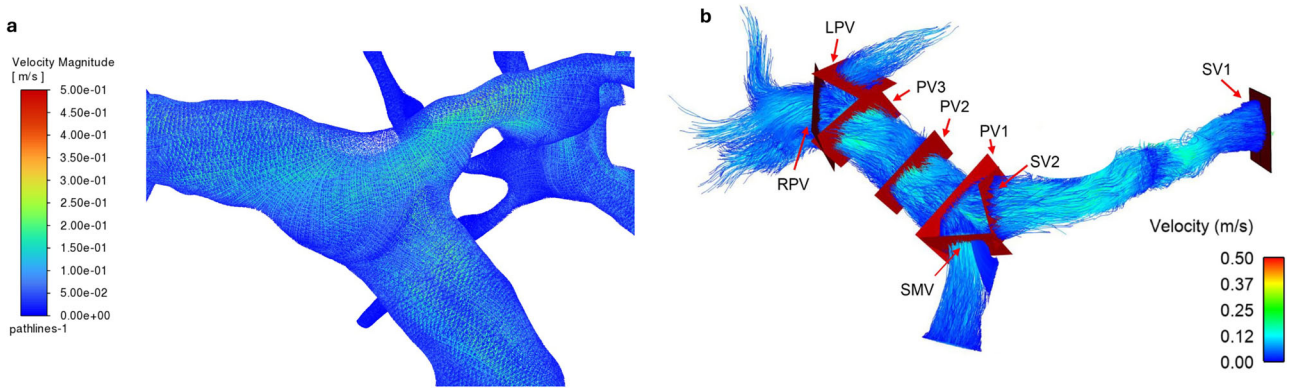


Fig. 4 | Comparison of simulation CFD results of the PV with 4D MRI flow. a PV velocity magnitude (m/s) predicted with multi-scale pipeline. **b** PV velocity magnitude (m/s) predicted measured with 4D MRI flow from Huang et al.[55].

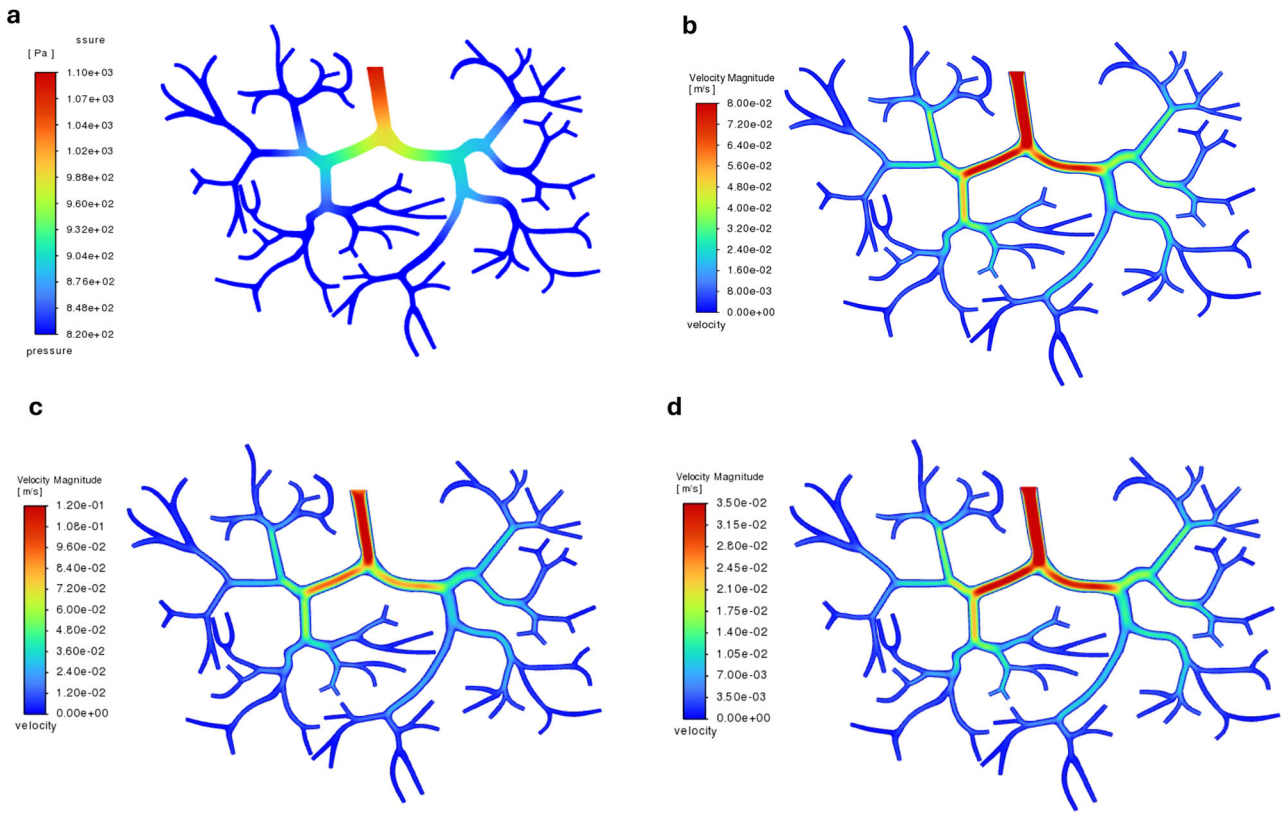


Fig. 6 | Large CSM CFD simulation results. a Pressure scheme (Pa). **b** Average inlet Velocity of 0.078 (m/s). **c** high inlet velocity of 0.12 (m/s). **d** Low inlet velocity of 0.035 (m/s).

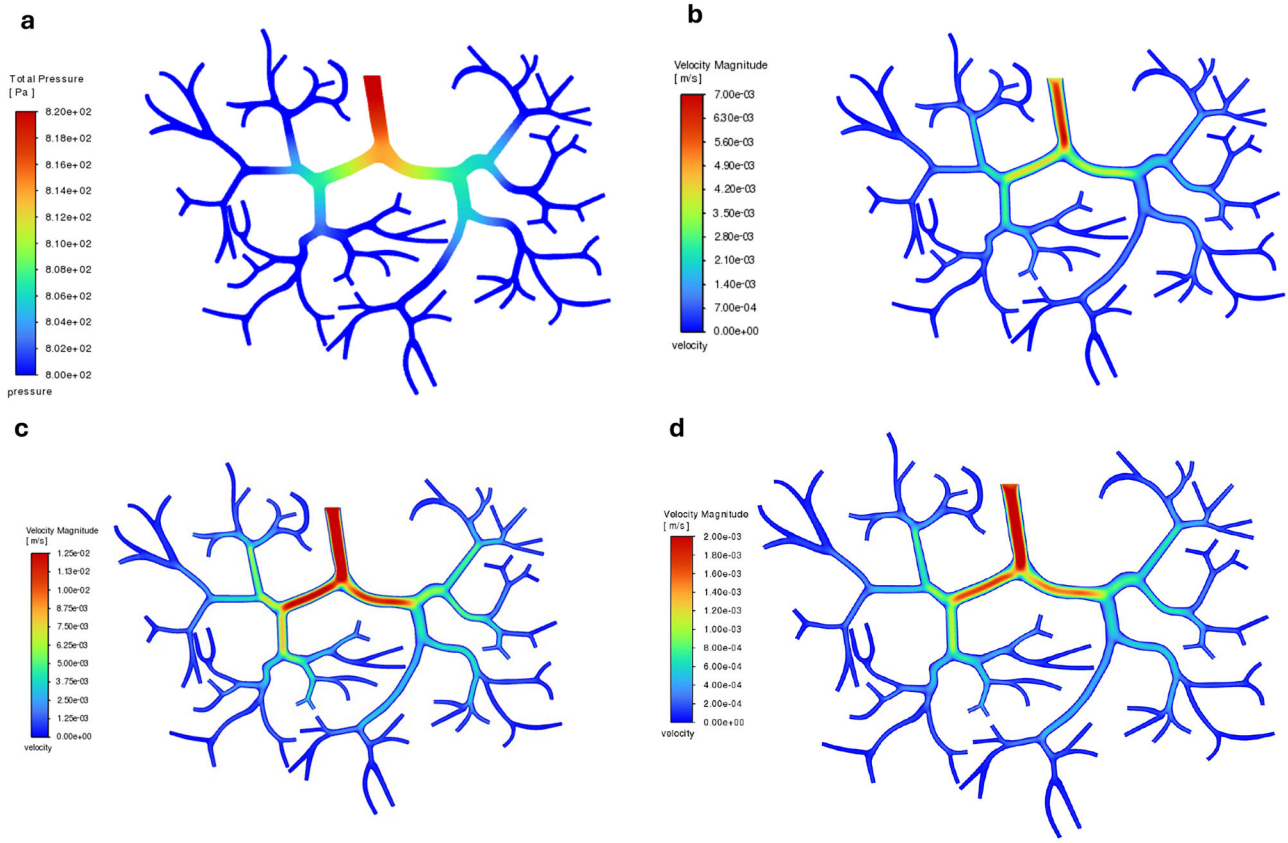


Fig. 7 | Small CSM CFD simulation results. a Pressure scheme (Pa). **b** Average inlet Velocity of 7.2 (mm/s). **c** High inlet velocity of 12.5 (mm/s). **d** Low inlet velocity of 2 (mm/s).

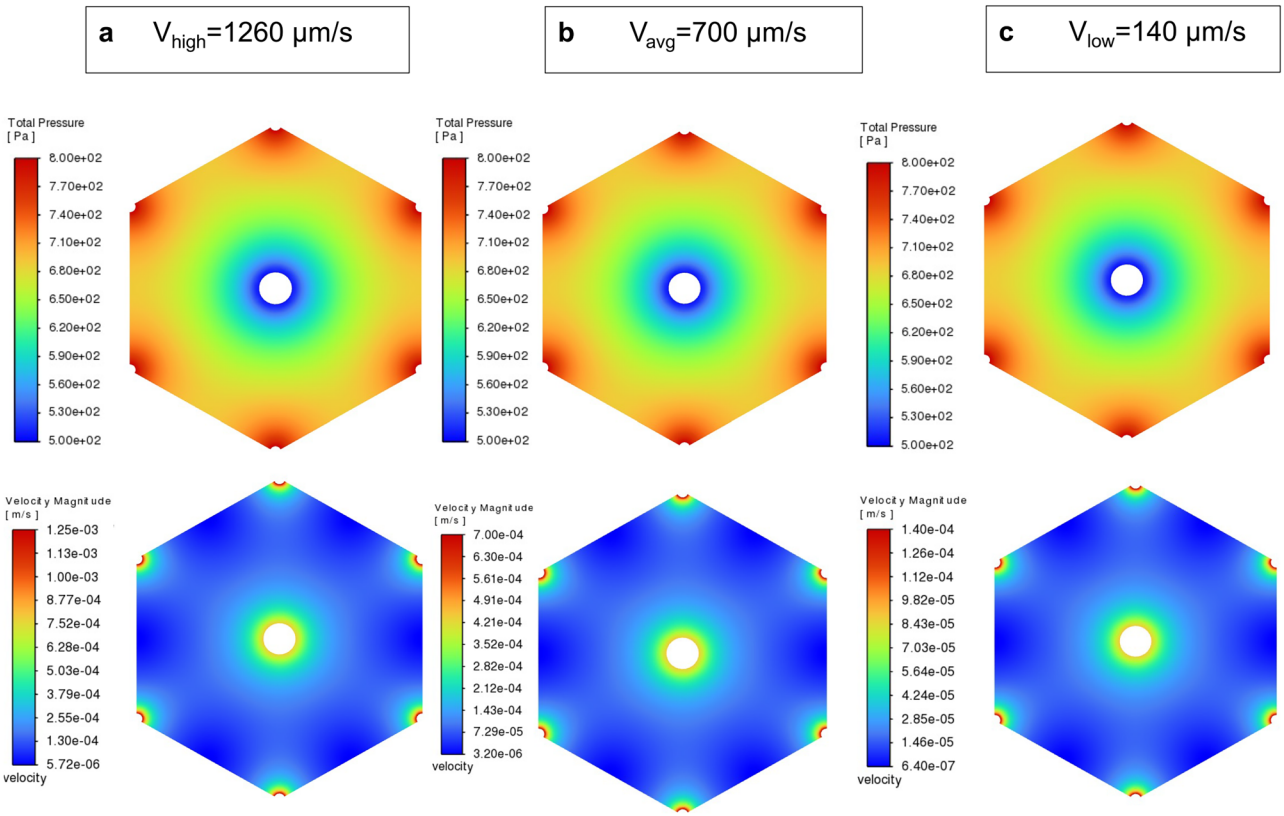


Fig. 8 | Lobule CFD simulation results. a High velocity. **b** Average velocity. **c** Low velocity inlet of both pressure and velocity inside the lobule.

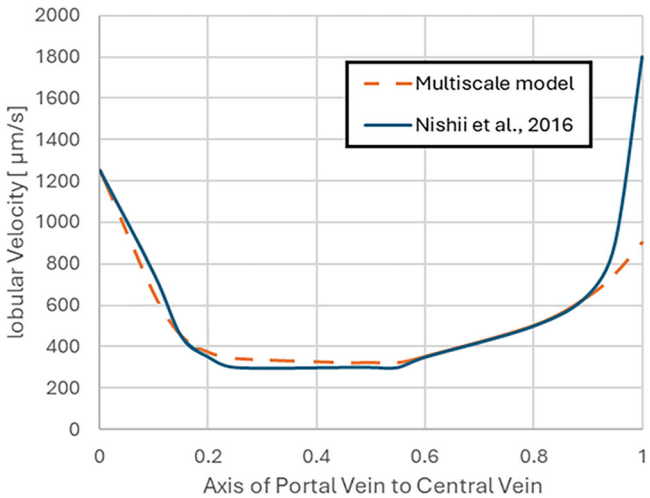


Fig. 9 | Validation of lobular velocity profile against literature data. Velocity along the portal-to-central vein axis within the lobule is shown for the multiscale model (dashed orange) and experimental data from Nishii et al. (solid blue).

right liver lobe. These findings highlight the importance of accounting for regional variability to predict drug intake and flow distribution accurately.

The CSM successfully generated detailed flow data for approximately 100,000 lobule outlets, connecting macro portal vein dynamics to micro sinusoidal flows. This scalability allows the integration of numerous lobules, enabling predictions of how localized lobular damage impacts overall liver health. Expanding to the general scope of DILI, the model captures critical feedback loops, where damaged lobules can increase local vascular resistance, which leads to blood flow redistribution. By incorporating spatial heterogeneity, the CSM offers valuable insights into liver dynamics under stress conditions, including portal hypertension and DILI.

Lobule simulations provided detailed insights into how drug flow, porous media permeability, and velocity affect drug delivery and tissue damage within the lobules. Simulations revealed a linear relationship between inlet velocity and flow within the porous lobule tissue, with velocities ranging from 60 to 600 µm/s, consistent with experimental data[53,63]. The alignment of the porous media permeability parameters with published results validated the model's accuracy. The virtual lobule damage model, based on prior work[11], also reproduced patterns of APAP-induced injury. Furthermore, the simulations demonstrated that even with the velocity spatial heterogeneity, a single episode of AILI does not significantly alter drug distribution dynamics, as hepatocytes have taken up nearly all the APAP before injury and necrosis occur. By incorporating spatial variability and feedback mechanisms, this model advances understanding of liver injury progression and provides a robust foundation for further work toward a goal of personalized medicine. The integration of patient-specific anatomical and clinical data enables tailored simulations, dynamically predicting liver responses to drugs based on individual physiology. This approach offers significant potential for improving therapeutic strategies for DILI, other liver diseases, and the genesis and progression of portal hypertension due to cirrhosis.

Despite its strengths, the current model has limitations that can be addressed by future refinements. Static boundary conditions may not fully capture dynamic changes in blood flow and vascular resistance during injury progression. Incorporating adaptive boundary conditions that evolve in real time could address this limitation. Additionally, the model employs a 2D planar capillary surrogate to simplify bifurcation structures and steady-state flow. While this preserves key geometric features, it does not fully capture three-dimensional microvascular dynamics or local permeability variations due to fibrosis or inflammation. Drug transport is also simplified, excluding active transport mechanisms. Future refinements will explore 3D reconstructions and dynamic permeability changes to enhance predictive accuracy.

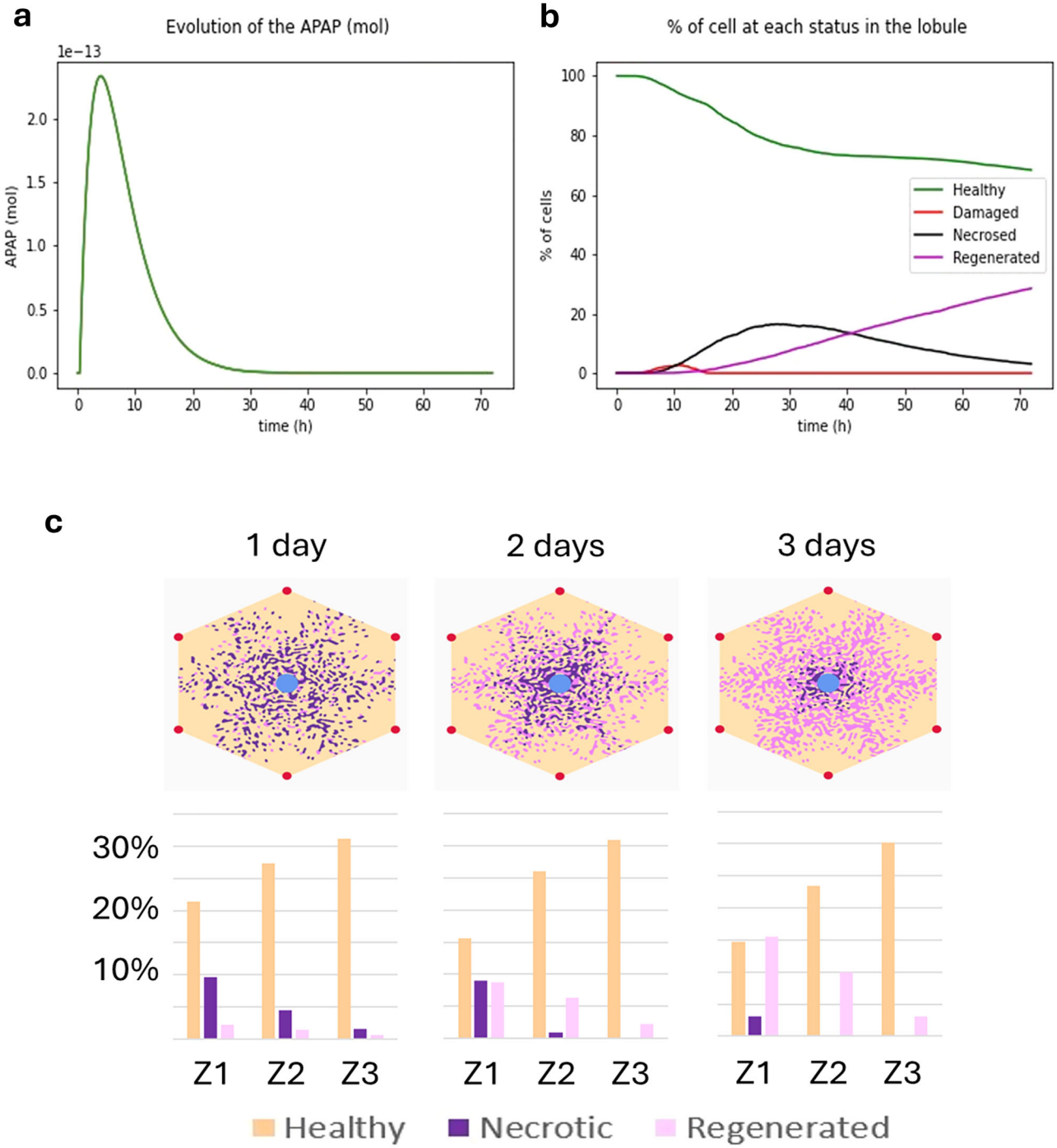


Fig. 10 | Results obtained for a 27.1 g overdose. a Lobule cellular APAP input obtained for a 27.1 g overdose. **b** Induced proportion of cellular states in the lobule during overdose. **c** Resulting lobular damage map for the scenario.

While the model effectively captures vascular inflow heterogeneity from the portal vein, it needs to be further refined to capture the hepatic artery (approximately 20% of the total lobular flow) and hepatic vein flow to fully address inflow and especially drainage of the HLVT. To enhance physiological realism, future extensions will also incorporate lymph formation and flow. These future refinements will allow us to capture crucial cellular-level processes—inflammation, immune responses, and endothelial injury—and hold the potential to leverage the HLVT beyond DILI toward liver disease.

This study demonstrates the successful integration of multiscale simulations, bridging the gap between organ- and lobule-level dynamics. The model accurately captures blood flow across the portal vein up to its smallest capillaries and predicts drug absorption processes across scales. We address the limitations of earlier single-scale models—some focused on large-scale vascular hemodynamics, others on small-scale lobular transport—by unifying macro (portal vein), mesoscale (capillaries), and micro (lobules) within one patient-specific framework. This integration enables the first CFD-based simulation of drug-induced liver injury that simultaneously spans these critical scales. It provides a robust and scalable framework for investigating liver function and drug-induced damage. Incorporating patient-specific data further enhances its relevance for clinical and pharmaceutical applications, paving the way for personalized treatment strategies and advancing the understanding of liver disease and therapy. As the model evolves, and the Living Liver initiative grows, it holds the potential

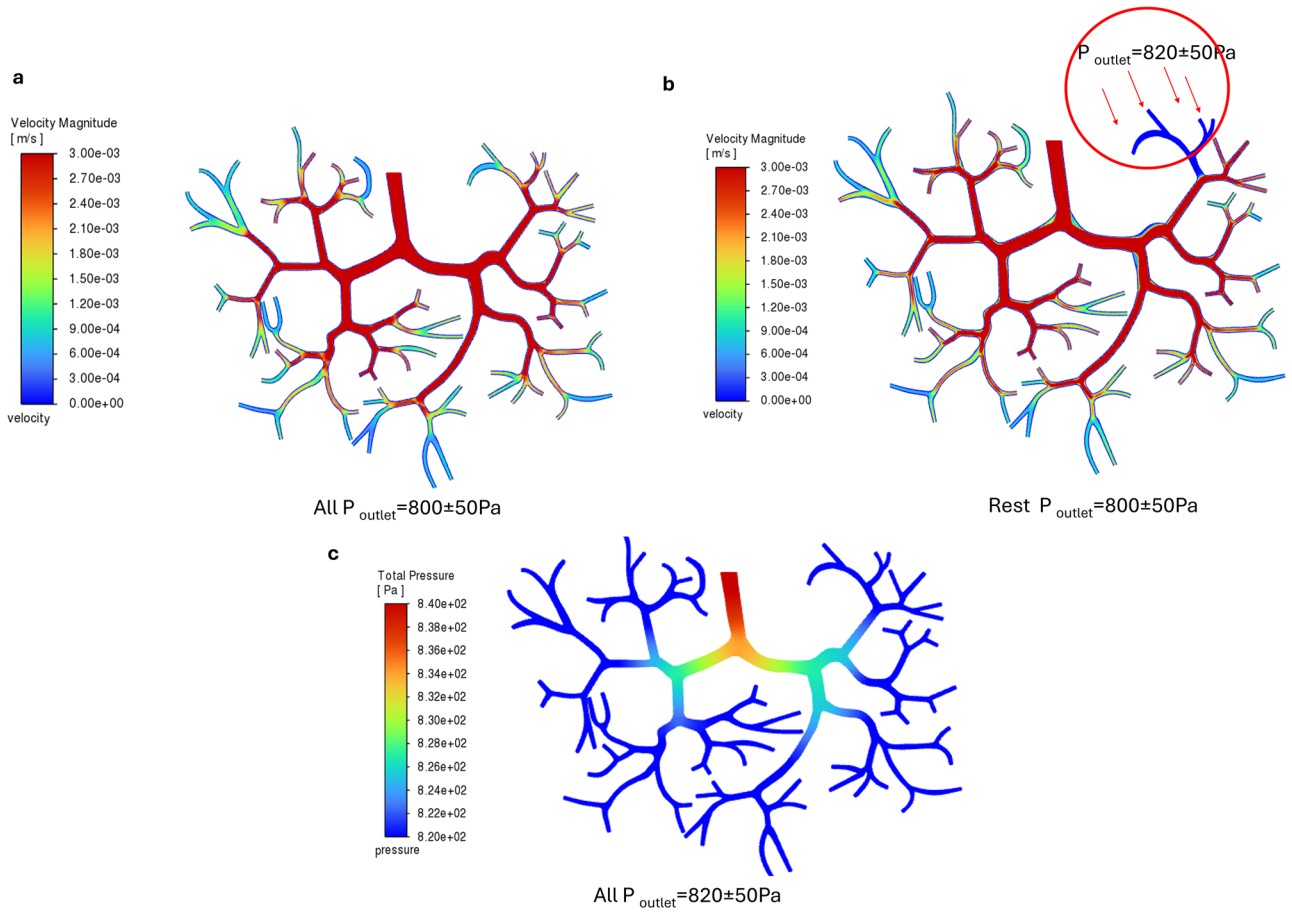


Fig. 11 | Simulated DILI synthetic scenarios progression under varying lobular damage conditions. 2 mm/s velocity inlet of L-CSM model results. **a** Normal healthy capillary. **b** 1–4 outlets section (marked in red) that has damaged lobules with 820 Pa high-pressure. **c** All lobules are damaged with 820 Pa high pressure All 820 Pa.

to transform the development and clinical application of novel therapeutics, improving precision, efficacy and safety.

Material and methods

MRI Data

A standard 1.5 Tesla magnetic MRI scan of the patient's liver was performed with gadolinium contrast enhancement. Fast breath-hold T1 and T2 sequences are obtained, with additional diffusion-weighted imaging used for further structural characterization. The images are obtained in Digital Imaging and Communications in Medicine (DICOM) standard and exported to a separate semi-autonomous segmentation software (LiverVision™, Medivision Ankara, Türkiye). LiverVision segments different structures within the DICOM images using sensitivity thresholding based on pixel brightness and avidity. The post-segmentation images are then rendered into 3D images using stereolithography or standard tessellation language (STL) format. The STL surfaces were smoothed and joined to a full 3D solid model to avoid small elements and all inlets and outlets were cut perpendicular to the vein diameter to obtain accurate results.

Ethics statement

Patient consent was not obtained because data was retrospective, based on standard care, and was analyzed anonymously[64]. The protocol was approved by the Institutional Review Board of the National University Hospital of Singapore in accordance with the Declaration of Helsinki (reference number 2020/01044).

Multiscale modeling

We developed a methodology to address the variations in both time and spatial scales from the liver (organ), lobule (unit) and hepatocyte (cellular) levels (Fig. 12). These models span several orders of magnitude, both temporally as APAP absorption occurs over hours to days while blood flow and drug transport occur in seconds or less, and spatially with the organ level (10 cm) to lobules (1 mm) and hepatocytes (microns). Bridging these differences requires a multiscale integration framework, detailed below.

The liver's spatial and temporal scales present challenges for multiscale modeling of DILI. At the organ scale (Fig. 13A), the liver geometry is derived from patient-specific CT/MRI scans. Blood flow in major vessels, ranging from 100 mm to 1.5 mm in diameter, is modeled using CFD simulations. The drug input was defined to represent drug diffusion in the blood after absorption by the guts. This provides the model with clinically relevant to APAP concentration evolution. The mesoscale (Fig. 13b), spanning 1.5 mm to 50 microns, focuses on capillaries and smaller vessels, where resolution limitations of CT/MRI necessitate the use of a surrogate CFD model. This mesoscale model generates 100,000 data points of outlet velocity and concentration, which serve as inputs for the lobule scale (Fig. 13c). At the lobule scale, the liver's functional units are modeled to incorporate blood flow and APAP transport into hepatocytes, as described by Camara Dit Pinto et al.[11]. These simulations refine predictions of cellular damage caused by APAP (Fig. 13d).

The process of linking models with different timescales is called temporal integration. At the organ level, drug absorption happens over hours or days, while blood flow simulations focus on changes that occur in seconds. To connect these scales, drug concentrations entering the blood vessels are broken into small intervals and analyzed in 5-s steps. These velocities and concentrations are then used to set boundary conditions for smaller-scale models of the liver, which capture APAP transport and hepatocyte damage dynamics to simulate how the drug spreads and causes cell damage, using 20-minute steps. Spatial integration ensures that information flows

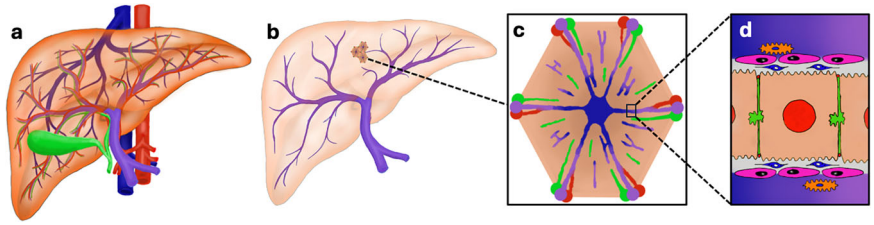


Fig. 12 | Visualization of the different scales of the human liver. The organ scale (cm) with (**a**) the liver and (**b**) the portal vasculature. **c** The functional scale (mm), the lobule and (**d**) the cellular scale (μm) with hepatocytes in beige, stellate cells in blue, Kupfer cells in orange and endothelial cells in pink. Figure adapted from Camara Dit Pinto et. al.[11] with authorization.

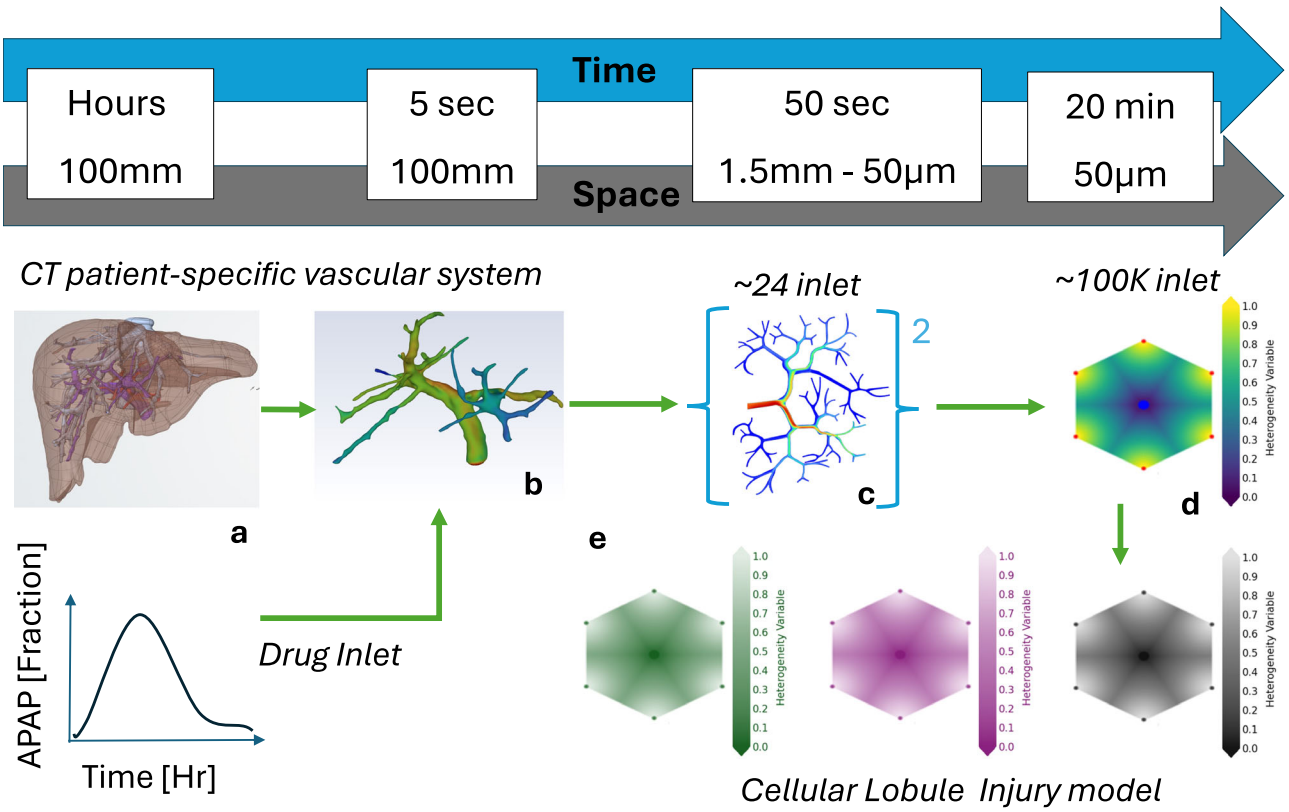


Fig. 13 | Multiscale methodology. a Introduction of patient-specific Portal Vien from MRI and APAP drug time concertation from PBPK models. **b** CFD simulations of Portal Vien. **c** CFD simulation of Large and Small capillaries model. **d** CFD Lobule models. **e**Schematic view of lobule Damage model.

smoothly between models of different sizes. Large-scale models of the liver provide data on blood flow and drug concentration directly to medium-scale simulations, which then refine this information for smaller-scale models of the liver's functional units. Boundary conditions at each scale are iteratively updated based on feedback from the others (Fig. 5). This approach connects the big picture (how the liver absorbs drugs) with the details (how liver cells are damaged).

The multiscale drug pipeline integrates blood flow and cellular injury models to simulate APAP-induced liver damage (Fig. 13), building on previously reported methods[11] with a key modification: boundary conditions from the portal vein are now introduced via CFD simulations. The pipeline has two main components: (1) blood flow simulation with APAP transport and (2) a cellular injury model, which run iteratively to simulate the progression of injury within the lobule. First, healthy blood flow is modeled using a species transport and advection-diffusion framework to track APAP concentration throughout the lobular blood flow. The cellular injury model then evaluates the impact of the drug at each node of the computational mesh, determining health status node by node. Simulations are conducted using a transient, pressure-based Navier-Stokes solver, enhanced with Python scripts to incorporate specific parameters outlined in Table 1. While the current pipeline is parameterized for APAP, it can be adapted to assess the effects of other drugs and treatments. For this model, drug diffusion from the gut into the bloodstream is specified to follow a predictable timeline: diffusion begins immediately after ingestion, reaching peak concentrations at 3 hours, averaging at 6 hours, and dropping to undetectable levels by 8 hours. This structured framework enables the dynamic simulation of APAP transport and injury progression within the liver.

Blood flow simulation with drug transport and Boundary conditions

Blood flow simulations across three scales were performed using a transient, pressure-based solver. Portal venous flow is typically modeled as steady-state; however, this study employs a transient solver to capture pulsatile hepatic inflow, better reflecting physiological dynamics, especially in pathological states like fibrosis, cirrhosis, or drug-induced vascular changes. While drug transport was modeled using a species transport framework to ensure accurate mass fractions of drug to blood within each element. To account for the non-Newtonian behavior of blood, the Carreau model for shear-thinning viscosity was applied at the capillary and lobule scales[65]. This model captures the variation in blood viscosity with shear rate, particularly in regions with high velocity gradients, enabling realistic simulation of pressure differences and velocity distributions. Parameters for the Carreau model were drawn from established blood flow modeling literature[66] and are

Table 1 | Blood flow and drug transport model parameters for each scale

Simulation	Parameter	Value	Reference
All Simulations	Permeability	1.0×10^{-14} to 1.0×10^{-15} [m^2]	53
	Blood density	1050 [kg/m^3]	53
	APAP drug density	1260 [kg/m^3]	69
	Blood Mw	64,500 [kg/kmol]	70
	APAP drug Mw	151.1 [Kg/kmol]	69
	Mixture mass diffusivity	2.22×10^{-10} [m^2/s]	71
Viscosity model (Blood/APAP)	Zero-shear viscosity	0.056 [Pa s]	66
	Infinite-shear viscosity	0.00345 [Pa s]	
	Time constant	1.902 [s]	
	Power-law index(n)	0.22	
Organ Scale Portal Vein Simulation	Inlet diameter	10.8[mm]	Patient data
	Outlet diameter	1.5-3.5 [mm]	Patient data
	Flow rate inlet	9.48-11.43[cm^3/s]	52
	Pressure outlet	1100 ± 50 [Pa]	Tailored to fit
Capillary Surrogate Model (CSM) Simulation	Diameter Large SCM	1.5[mm] to 0.3[mm]	From upper scale
	Diameter Small SCM	0.3[mm] to 50[μm]	From upper scale
	Flow rate inlet	From Upper scale	From Upper scale
	Large CSM Pressure outlet	820 ± 50 [Pa]	Tailored to fit
	Small CSM Pressure outlet	800 ± 50 [Pa]	53
Virtual Lobule Simulation	Portal Track diameter	0.05 [mm]	59
	Central Vein diameter	0.15 [mm]	53
	Lobule diameter	1.5 [mm]	53
	Flow rate inlet	From upper scale	From upper scale
	Pressure outlet	660 [Pa]	53

detailed in Table 1. The viscous model ensures that shear-rate-dependent viscosity is accurately represented in areas with varying velocities.

Boundary conditions were tailored to maintain fluid dynamic continuity across scales. Inlet velocities, fitted from Ma et al.[52], determined the inlet pressures, as shown in Fig. 2. Outlet boundary conditions at each scale were calculated to match the average outlet velocity from the previous scale to the resulting inlet pressure of the current scale. This approach ensured consistent transitions in fluid dynamics down to the lobule level, where inlet pressure was set at approximately 800 Pa[53]. The outlet pressures for each scale are summarized in Table 1, with a pressure span of ±50 Pa based on initial conditions in Fig. 2. This span remained consistent across boundary conditions, and velocity spans were verified to align with the resulting pressure spans, ensuring accurate simulation across all scales.

To ensure accurate inflow and outflow boundary conditions, the portal vasculature geometry was trimmed at the inlet and outlet to create smooth surfaces. A 3D simulation was constructed based on the refined geometry, capturing the complex vein structure and varying diameters, as shown in Fig. 1. The mesh used an element size of 5×10^{-4} m, resulting in approximately 1 million elements. The vascular outlet diameters ranged from 3.5 mm to 1.5 mm, matching typical MR angiography resolution limit. The portal vein inlet flow rate varied between 9.48 cm^3/s and 11.43 cm^3/s in a one-second cycle, as shown in Fig. 2, replicating the dynamics of heart-driven blood flow into the portal vein[52]. All 24 outlets were assigned a default pressure of 1100 ± 50 Pa to ensure compatibility with the models of veins below 1.5 mm in diameter. Simulations were run until a dynamic equilibrium of outlet velocities and drug concentration was achieved. A fixed time step of 0.001 s was applied after an initial relaxation phase with five steps of 1×10^{-5} seconds. The simulation duration was set to 100 s, sufficient to ensure stabilization of both drug transport and outlet velocities. Results were verified for convergence with respect to both mesh size and time step.

APAP drug concentrations varied to follow evolution clinically observed during drug ingestion, with simulations exploring concentrations from 0 to 8e−3 kg/L to model different dosages over specific time intervals[67]. It is important to note that the simulation included only blood flow, drug transport, and their mixture, without modeling any biological or chemical reactions.

The Capillary Surrogate Model (CSM) was developed to bridge the spatial gap between MR resolution limit and the liver lobule. Using the Constrained Constructive Optimization (CCO) approach[68], the CSM generates approximately 10,000 individual outlets to the lobule scale. The model begins with an inlet diameter of 1.5 mm and extends to outlets as small as 50 microns, effectively connecting the macro (organ-level) and micro (lobule-level) scales. To enable hundreds of computational runs while preserving critical vascular structures, the Capillary Surrogate Model (CSM) was implemented as a 2D planar simulation. This approach preserves key structural details such as bifurcation angles, segment lengths, and diameters while allowing for sensitivity analyses and efficient flow dynamic studies. However, a key limitation of this 2D approach is that it prevents vessel crossings, which can affect local perfusion distributions compared to an in vivo 3D vascular network. While this simplification does not fully replicate complex 3D hepatic vasculature, it allows for controlled sensitivity testing of hemodynamic parameters and can be extended to 3D models where computational feasibility permits. The CSM includes two configurations: the Large CSM and the Small CSM. The Large CSM represents a vascular segment with inlets of 1.5 mm and outlets of 0.3 mm, while the Small CSM scales down to inlets of 0.33 mm and outlets of 50 microns. Both models approximate blood flow behavior rather than providing precise, patient-specific results, serving as an efficient surrogate to capture flow dynamics. This is readily extendable to 3D models, provided the impact of various configurations on simulation outcomes and sensitivity analyses justifies the additional computation burden.

For the Large CSM, a mesh element size of 1.1×10^{-4} m was used, generating 70,000 elements. Inlet velocities ranged from 0.04 to 0.12 m/s, based on outputs from the 3D portal vein simulation. The outlets were assigned a default pressure of 830 ± 20 Pa, ensuring compatibility with downstream models for veins below 0.3 mm. In the Small CSM, a finer mesh element size of 2×10^{-5} m was applied, resulting in the same number of elements. Inlet velocities ranged from 0.004 to 0.04 m/s, with outlets set to a default pressure of 800 ± 20 Pa, aligning with lobule vein inlet conditions[53]. Both models were run until dynamic equilibrium of outlet velocities and drug concentrations was achieved. Simulations used a fixed timestep of 0.001 seconds, following an initial relaxation phase with five timesteps of 1×10^{-5} seconds. Simulation durations ranged from 10 to 100 s, ensuring stabilization of both velocity and APAP concentration throughout the veins and outlets. Convergence was verified with respect to both mesh size and time step, confirming the reliability of the results. This 2D surrogate modeling framework efficiently captures small vein flow and drug transport dynamics, providing a scalable tool to bridge the macroscopic and microscopic scales in liver modeling. While simplified, the CSM effectively complements lobule-level models and lays the groundwork for future exploration of 3D implementations and patient-specific configurations.

The lobule simulations were based on a 2D representation of the liver lobule, following methodologies from previous work[11]. A mesh element size of 1.75×10^{-5} m was used, resulting in approximately 60,000 elements. Boundary conditions were derived from capillary-scale simulations, with inlet velocities corresponding to portal vein outlet data and outlet pressure set to 500 ± 20 Pa[53]. These conditions modeled normal blood flow across various portal vein outlets. A critical factor in the lobule simulation was the permeability of the porous media, which directly influenced internal velocities and pressures. Transitioning from the smooth, nonporous vascular system to the porous lobule, which encompasses both vasculature and tissue, required careful tailoring of boundary conditions. The permeability was adjusted to align the inlet pressure of 800 Pa with the outlet pressure of 500 Pa, ensuring consistent fluid dynamics across scales[51,53]. The simulation ran until dynamic equilibrium of outlet velocities and drug concentrations was achieved. A fixed timestep of 1 s was used, and simulations were run for 20 min to evaluate the progression of APAP-induced damage. Each cell in the lobule model represented hepatic arterial tissue and computed the concentration of APAP, providing data for assessing cellular injury. To model APAP-induced injury, a modified MALD damage model was employed, consistent with previous lobule simulation studies[11]. This model linked drug concentration in tissue cells to corresponding levels of cellular damage, enabling an evaluation of injury evolution within the lobule. The integration of these simulations allowed for detailed insight into the dynamics of APAP transport and hepatocyte damage at the cellular level.

Modeling patient conditions

The developed multiscale liver platform presented in this work opens the door to predicting hemodynamic changes based on patient pathologies. To showcase those capabilities, two scenarios were created. The first scenario recreates the effects of hepatocellular necrosis with injury to liver sinusoidal endothelial cells and/or endothelia of the central veins (i.e., sinusoidal obstructive syndrome). In this first scenario, an outlet pressure increase in a specific section of the small CSM is applied with the aim of reducing the blood flow to a negligible value (inducing limited drug transport in the affected lobules). The second scenario aims to recreate the effects of veinous pressure increase due to vena cava obstruction. In this second scenario, an outlet pressure increase is applied to the whole small CSM outlets. These scenarios do not represent specific known or observed clinical conditions, but are fictitious scenarios created to test the robustness of the model and explore possible theories.

Data availability

Segmented vasculature files can be made available upon reasonable request.

Code availability

ANSYS Fluent simulation files can be made available upon reasonable request.

Received: 22 January 2025; Accepted: 20 May 2025;
Published online: 23 June 2025

References

1. Hosack, T., Damry, D. & Biswas, S. Drug-induced liver injury: a comprehensive review. *Ther. Adv. Gastroenterol.* **16**, 17562848231163410 (2023).
2. Andrade, R. J. et al. Drug-induced liver injury. *Nat. Rev. Dis. Prim.* **5**, 58 (2019).
3. Mostafa, F. & Chen, M. Computational models for predicting liver toxicity in the deep learning era. *Front Toxicol.* **5**, 1340860 (2023).
4. Ellison, C., Hewitt, M. & Przybylak, K. In Silico Models for Hepatotoxicity. *Methods Mol. Biol.* **2425**, 355–392 (2022).
5. Speid, L. H., Lumley, C. E. & Walker, S. R. Harmonization of guidelines for toxicity testing of pharmaceuticals by 1992. *Regulatory Toxicol. Pharmacol.* **12**, 179–211 (1990).
6. Mulliner, D. et al. Computational models for human and animal hepatotoxicity with a global application scope. *Chem. Res. Toxicol.* **29**, 757–767 (2016).
7. Xu, Z. et al. Research on the Species Difference of the Hepatotoxicity of Medicine Based on Transcriptome. *Front. Pharmacol*. **12** (2021).
8. Mitchell, S. J. & Hilmer, S. N. Drug-induced liver injury in older adults. *Therapeutic Adv. Drug Saf.* **1**, 65–77 (2010).
9. Shanks, N., Greek, R. & Greek, J. Are animal models predictive for humans?. *Philos., Ethics, Humanities Med.* **4**, 2 (2009).
10. Olson, H. et al. Concordance of the toxicity of pharmaceuticals in humans and in animals. *Regulatory Toxicol. Pharmacol.* **32**, 56–67 (2000).
11. Camara Dit Pinto, S. et al. A virtual scalable model of the Hepatic Lobule for acetaminophen hepatotoxicity prediction. *npj Digit. Med.* **7**, 340 (2024).
12. Esmailie, F. et al. Biomechanics of transcatheter aortic valve replacement complications and computational predictive modeling. *Struct. Heart* **6**, 100032 (2022).
13. Dowling, C., Gooley, R., McCormick, L., Firoozi, S. & Brecker, S. J. Patient-specific computer simulation: an emerging technology for guiding the transcatheter treatment of patients with bicuspid aortic valve. *Inter. Cardiol.* **16**, e26 (2021).
14. Finotello, A., Morganti, S. & Auricchio, F. Finite element analysis of TAVI: Impact of native aortic root computational modeling strategies on simulation outcomes. *Med. Eng. Phys.* **47**, 2–12 (2017).
15. Astudillo, P., De Beule, M., Dambre, J. & Mortier, P. Towards safe and efficient preoperative planning of transcatheter mitral valve interventions. *Morphologie* **103**, 139–147 (2019).
16. Baillargeon, B., Rebelo, N., Fox, D. D., Taylor, R. L. & Kuhl, E. The Living Heart Project: a robust and integrative simulator for human heart function. *Eur. J. Mech. A: Solids* **48**, 38–47 (2014).
17. Flynn, D., Palmer, M., Schiestl, R., Levine, S. & Maeder, T. Medical Device Innovation Consortium (MDIC), Landscape report on medical device computational modeling and simulation for medical devices https://mdic.org/wp-content/uploads/2018/05/MDIC-CMS-Landscape-Report.pdf (2018).
18. Morrison, T. M., Dreher, M. L., Nagaraja, S., Angelone, L. M. & Kainz, W. The role of computational modeling and simulation in the total product life cycle of peripheral vascular devices. *J. Med. Device* **11**, 024503 (2017).
19. Badano, A. In silico imaging clinical trials: cheaper, faster, better, safer, and more scalable. *Trials* **22**, 64 (2021).
20. Avanzato, R., Beritelli, F., Lombardo, A. & Ricci, C. Lung-DT: an ai-powered digital twin framework for thoracic health monitoring and diagnosis. *Sensors* **24**, 958 (2024).

21. Zhu, L., Lu, W., Soleimani, M., Li, Z. & Zhang, M. Electrical impedance tomography guided by digital twins and deep learning for lung monitoring. *IEEE Trans. Instrum. Meas.* **72**, 1–9 (2023).
22. Hurtado, D. E., Avilés-Rojas, N. & Concha, F. Multiscale modeling of lung mechanics: From alveolar microstructure to pulmonary function. *J. Mech. Phys. Solids* **179**, 105364 (2023).
23. Weickenmeier, J., Butler, C. A. M., Young, P. G., Goriely, A. & Kuhl, E. The mechanics of decompressive craniectomy: personalized simulations. *Comput. Methods Appl. Mech. Eng.* **314**, 180–195 (2017).
24. Xiong, H. et al. The digital twin brain: a bridge between biological and artificial intelligence. *Intell. Comput.* **2**, 0055 (2023).
25. Sasikaladevi, N. & Revathi, A. Digital twin of renal system with CT-radiography for the early diagnosis of chronic kidney diseases. *Biomed. Signal Process. Control* **88**, 105632 (2024).
26. National Academies of Sciences, Engineering, and Medicine. In: *Opportunities and Challenges for Digital Twins in Biomedical Research: Proceedings of a Workshop-in Brief. in 26922* (National Academies Press, Washington, D.C., 2023). https://doi.org/10.17226/26922.
27. Ho, H., Rezania, V. & Schwen, L. O. Editorial: Multiscale modeling for the liver. *Front. Bioeng. Biotechnol.* **11** (2023).
28. Schwen, L. O., Kuepfer, L. & Preusser, T. Modeling approaches for hepatic spatial heterogeneity in pharmacokinetic simulations. *Drug Discov. Today.: Dis. Models* **22**, 35–43 (2016).
29. Karcaaltincaba, M. & Akhan, O. Imaging of hepatic steatosis and fatty sparing. *Eur. J. Radiol.* **61**, 33–43 (2007).
30. Goldstein, N. S., Hastah, F., Galan, M. V. & Gordon, S. C. Fibrosis heterogeneity in nonalcoholic steatohepatitis and hepatitis c virus needle core biopsy specimens. *Am. J. Clin. Pathol.* **123**, 382–387 (2005).
31. Avila, M. A. et al. Reduced mRNA abundance of the main enzymes involved in methionine metabolism in human liver cirrhosis and hepatocellular carcinoma. *J. Hepatol.* **33**, 907–914 (2000).
32. Xie, C. et al. Quantification of hepatic vascular and parenchymal regeneration in mice. *PLoS ONE* **11**, e0160581 (2016).
33. Gasselhuber, A. et al. Targeted drug delivery by high intensity focused ultrasound mediated hyperthermia combined with temperature-sensitive liposomes: Computational modelling and preliminary in vivovalidation. *Int. J. Hyperth.* **28**, 337–348 (2012).
34. Tanaka, T. et al. Radiologic placement of side-hole catheter with tip fixation for hepatic arterial infusion chemotherapy. *J. Vasc. Interventional Radiol.* **14**, 63–68 (2003).
35. Gasselhuber, A. et al. Mathematical spatio-temporal model of drug delivery from low temperature sensitive liposomes during radiofrequency tumour ablation. *Int. J. Hyperth.* **26**, 499–513 (2010).
36. Brennan, P. N., Cartlidge, P., Manship, T. & Dillon, J. F. Guideline review: EASL clinical practice guidelines: drug-induced liver injury (DILI). *Frontline Gastroenterol.* **13**, 332–336 (2022).
37. Guillot, A. & Tacke, F. Spatial dimension of macrophage heterogeneity in liver diseases. *egastro* **1** (2023).
38. Jaeschke, H. & Ramachandran, A. Acetaminophen hepatotoxicity: paradigm for understanding mechanisms of drug-induced liver injury. *Annu. Rev. Pathol.: Mech. Dis.* **19**, 453–478 (2024).
39. Chidiac, A. S., Buckley, N. A., Noghrehchi, F. & Cairns, R. Paracetamol (acetaminophen) overdose and hepatotoxicity: mechanism, treatment, prevention measures, and estimates of burden of disease. *Expert Opin. Drug Metab. Toxicol.* **19**, 297–317 (2023).
40. Li, X., Tang, J. & Mao, Y. Incidence and risk factors of drug-induced liver injury. *Liver Int.* **42**, 1999–2014 (2022).
41. Mehrpour, O., Saeedi, F., Hadianfar, A., Mégarbane, B. & Hoyte, C. Prognostic factors of acetaminophen exposure in the United States: An analysis of 39,000 patients. *Hum. Exp. Toxicol.* **40**, S814–S825 (2021).
42. Coombe, D., Rezania, V. & Tuszynski, J. A. Dual continuum upscaling of liver lobule flow and metabolism to the full organ scale. *Frontiers in Systems Biology* **2** (2022).
43. Rezania, V., Marsh, R., Coombe, D. & Tuszynski, J. A physiologically-based flow network model for hepatic drug elimination I: regular lattice lobule model. *Theor. Biol. Med Model* **10**, 52 (2013).
44. Rezania, V., Marsh, R., Coombe, D. & Tuszynski, J. A physiologically-based flow network model for hepatic drug elimination II: variable lattice lobule models. *Theor. Biol. Med. Model* **10**, 53 (2013).
45. Rezania, V., Coombe, D. & Tuszynski, J. A. A physiologically-based flow network model for hepatic drug elimination III: 2D/3D DLA lobule models. *Theor. Biol. Med. Model* **13**, 9 (2016).
46. Bonfiglio, A., Leungchavaphongse, K., Repetto, R. & Siggers, J. H. Mathematical modeling of the circulation in the liver lobule. *J. Biomech. Eng.* **132** (2010).
47. Mosharaf-Dehkordi, M. A fully coupled porous media and channels flow approach for simulation of blood and bile flow through the liver lobules. *Comput. Methods Biomech. Biomed. Eng.* **22**, 901–915 (2019).
48. Lambers, L. et al. Quantifying fat zonation in liver lobules: an integrated multiscale in-silico model combining disturbed microperfusion and fat metabolism via a continuum-biomechanical bi-scale, tri-phasic approach. *Biomech. Model. Mechanobiol* **23**, 631–653 (2023).
49. Gerhäusser, S. et al. Simulation of zonation-function relationships in the liver using coupled multiscale models: Application to drug-induced liver injury. Preprint at https://doi.org/10.1101/2024.03.26.586870 (2024).
50. Schliess, F. et al. Integrated metabolic spatial-temporal model for the prediction of ammonia detoxification during liver damage and regeneration. *Hepatology* **60**, 2040–2051 (2014).
51. Debbaut, C. et al. A 3D porous media liver lobule model: the importance of vascular septa and anisotropic permeability for homogeneous perfusion. *Comput. Methods Biomech. Biomed. Eng.***17**, 1295–1310 (2014).
52. Ma, R. et al. Anatomically based simulation of hepatic perfusion in the human liver. *Int. J. Numer. Methods Biomed. Eng.* **35**, e3229 (2019).
53. Hu, J., Lü, S., Feng, S. & Long, M. Flow dynamics analyses of pathophysiological liver lobules using porous media theory. *Acta Mech. Sin.* **33**, 823–832 (2017).
54. Schwen, L. O. et al. Spatio-Temporal simulation of first pass drug perfusion in the liver. *PLoS Comput. Biol.* **10**, e1003499 (2014).
55. Huang, A. et al. Reference values for 4D flow magnetic resonance imaging of the portal venous system. *Abdom. Radio.* **48**, 2049–2059 (2023).
56. Rohan, E., Turjanicová, J. & Lukeš, V. Multiscale modelling and simulations of tissue perfusion using the Biot-Darcy-Brinkman model. *Comput. Struct.* **251**, 106404 (2021).
57. Sluka, J. P. et al. A liver-centric multiscale modeling framework for xenobiotics. *PLoS ONE* **11**, e0162428 (2016).
58. Diaz Ochoa, J. G. et al. A multi-scale modeling framework for individualized, spatiotemporal prediction of drug effects and toxicological risk. *Front. Pharmacol*. **3** (2013).
59. Siggers, J. H., Leungchavaphongse, K., Ho, C. H. & Repetto, R. Mathematical model of blood and interstitial flow and lymph production in the liver. *Biomech. Model Mechanobiol.* **13**, 363–378 (2014).
60. Nishii, K., Reese, G., Moran, E. C. & Sparks, J. L. Multiscale computational model of fluid flow and matrix deformation in decellularized liver. *J. Mech. Behav. Biomed. Mater.* **57**, 201–214 (2016).
61. George, S. M., Eckert, L. M., Martin, D. R. & Giddens, D. P. Hemodynamics in normal and diseased livers: application of image-based computational models. *Cardiovasc. Eng. Tech.* **6**, 80–91 (2015).

62. Roldán-Alzate, A. et al. Characterization of mesenteric and portal hemodynamics using 4D flow MRI: the effects of meals and diurnal variation. *Abdom. Radio.* **47**, 2106–2114 (2022).
63. Nakata, M. et al. Alterations to hepatic microcirculation in thioacetamide-induced cirrhotic livers of rats. *Osaka City Med. J.* **48**, 1–8 (2002).
64. Balci, D., Kirimker, E. O., Raptis, D. A., Gao, Y. & Kow, A. W. C. Uses of a dedicated 3D reconstruction software with augmented and mixed reality in planning and performing advanced liver surgery and living donor liver transplantation (with videos). *Hepatobiliary Pancreat. Dis. Int.* **21**, 455–461 (2022).
65. Yasuda, K., Armstrong, R. C. & Cohen, R. E. Shear flow properties of concentrated solutions of linear and star branched polystyrenes. *Rheol. Acta* **20**, 163–178 (1981).
66. Weddell, J. C., Kwack, J., Imoukhuede, P. I. & Masud, A. Hemodynamic analysis in an idealized artery tree: differences in wall shear stress between newtonian and non-newtonian blood models. *PLoS ONE* **10**, e0124575 (2015).
67. Remien, C. H., Adler, F. R., Waddoups, L., Box, T. D. & Sussman, N. L. Mathematical modeling of liver injury and dysfunction after acetaminophen overdose: early discrimination between survival and death. *Hepatology* **56**, 727–734 (2012).
68. Whitehead, J. F., Laeseke, P. F., Periyasamy, S., Speidel, M. A. & Wagner, M. G. In silico simulation of hepatic arteries: An open-source algorithm for efficient synthetic data generation. *Med. Phys.* **50**, 5505–5517 (2023).
69. PubChem. Acetaminophen. https://pubchem.ncbi.nlm.nih.gov/compound/1983.
70. Billett, H. H. in *Clinical Methods: The History, Physical, and Laboratory Examinations* (eds. Walker, H. K., Hall, W. D. & Hurst, J. W.) (Butterworths, 1990).
71. Ribeiro, A. et al. Diffusion coefficients of paracetamol in aqueous solutions. *J. Chem. Thermodyn.* **54**, 97–99 (2012).

Acknowledgements

The authors would like to thank the Long Island University-Dassault Systèmes Center of Excellence and the Baylor College of Medicine Learning Health System for their financial support.

Author contributions

N.R.G. supervised and led the project conceptualization and administration. A.M.M. performed the simulation setup, data collection, and curation. S.C.D.P. helped to implement parts of the computational pipeline, data collection, and data analysis. N.R.G., A.M.M. and S.C.D.P. analyzed the results and wrote the original draft. M.C., S.M.L., G.K.S., S.A., S.D., G.Y. and J.M.V. provided important clinical and computational intellectual content for the study design and results analysis. M.C., S.M.L., G.K.S., S.A., S.D., G.Y. and J.M.V. contributed to writing the final draft of the manuscript. All authors critically reviewed the paper and contributed important intellectual content. All authors have read and approved the manuscript.

Competing interests

S.M.L. is a Dassault Systemes employee. J.M.V. is a member of IQDILI and the NIH NIDDK Drug-Induced Liver Injury Network Data Safety and Management Board. N.R.G. has served as a consultant for Dassault Systemes. The remaining authors declare no competing interests.

Additional information

Correspondence and requests for materials should be addressed to Nicolas R. Gallo.

Reprints and permissions information is available at http://www.nature.com/reprints

Publisher's note Springer Nature remains neutral with regard to jurisdictional claims in published maps and institutional affiliations.
Additional information: Correspondence and requests for materials should be addressed to Nicolas R. Gallo.

Open Access This article is licensed under a Creative Commons Attribution-NonCommercial-NoDerivatives 4.0 International License, which permits any non-commercial use, sharing, distribution and reproduction in any medium or format, as long as you give appropriate credit to the original author(s) and the source, provide a link to the Creative Commons licence, and indicate if you modified the licensed material. You do not have permission under this licence to share adapted material derived from this article or parts of it. The images or other third party material in this article are included in the article's Creative Commons licence, unless indicated otherwise in a credit line to the material. If material is not included in the article's Creative Commons licence and your intended use is not permitted by statutory regulation or exceeds the permitted use, you will need to obtain permission directly from the copyright holder. To view a copy of this licence, visit http://creativecommons.org/licenses/by-nc-nd/4.0/.

© The Author(s) 2025